

Artificial Debris Collision Risk Following a Catastrophic Spacecraft Mishap in Lunar Orbit

Nathan R. Boone*

Air Force Institute of Technology

Robert A. Bettinger†

Air Force Institute of Technology

ABSTRACT

This research analyzes the effects of a catastrophic spacecraft mishap in a polar lunar orbit in terms of the risks posed to a notional lunar spacecraft operating in an Apollo-like, equatorial lunar orbit. Robust models for lunar trajectories, the survivability of spacecraft threatened by debris, and the vulnerability of spacecraft to debris are developed and used to quantify the risks from artificial lunar debris. The results of this research showed total one-month hazard probabilities on the order of about $10^{-3}\%$. While low, this probability could create some concern in real-world missions and may be comparable to the risk from debris in orbits near Earth. The majority of the debris particles had not decayed to the lunar surface by the end of the one-month simulation, which resulted in risk levels that did not diminish within one month. The results of this study demonstrate the need to consider debris mitigation strategies in lunar orbit, especially as more spacecraft begin to operate in this orbital environment.

1. INTRODUCTION

Over the past several years, as interest in lunar exploration has steadily increased, a variety of new space missions have operated in the lunar orbital region. These new space operations include a wide range of international missions to the Moon such as China's 2018 Chang'e-4 far side lunar lander, Israel's 2019 Beresheet mission, India's 2019 Chandrayaan-2 mission, and China's 2020 Chang'e-5 lunar sample return mission [1]. Furthermore, NASA plans to return humans to the Moon through the Artemis program within the next decade. The Artemis program aims to provide crewed landings on the Moon, lunar colonization, and a crewed space station in an orbit near the Moon called the Lunar Gateway. Increased interest in crewed exploration of the Moon is expected to lead to even greater numbers of spacecraft operating in the lunar region in the coming years [2].

As more spacecraft operate in the lunar region, the lunar space environment may become more crowded. This may require debris management techniques to avoid a potential "Kessler Syndrome," where a cascading series of collisions renders certain orbits unusable [3]. Artificial debris in Earth orbits has been heavily studied, but very few studies have examined the risks from artificial debris in orbits beyond Earth or around other celestial bodies. Debris in lunar orbit could be consequential due to small size of the Moon, which provides more opportunities for intersections with debris, and the lack of atmospheric drag around the Moon, which could cause particles to remain in orbit for extended periods of time. Although the non-spherical nature of the Moon's gravity can cause objects left in orbit to quickly decay to the surface, some lunar orbits are remarkably stable. A recent study by Meador [4] showed that the Apollo 11 Lunar Module Ascent Stage, which was left in lunar orbit in 1969, could remain in lunar orbit to this day. This example demonstrates the potential risk of artificial debris accumulation in lunar orbit.

This research aims to determine the effects of a significant artificial debris generating event in lunar orbit. The debris event was modeled as a catastrophic spacecraft battery explosion suffered by a spacecraft in a polar lunar orbit. The trajectories of the particles resulting from this mishap were propagated for one month using a high-precision lunar orbit propagator. A survivability model was then applied to analyze the debris collision risk to a spacecraft operating in an equatorial lunar orbit similar to that used by the Apollo missions. Overall, research into lunar debris propagation improves understanding of the relative importance of debris management in lunar orbit and the potential consequences of mishaps within this orbital regime.

*PhD Student, Air Force Institute of Technology, Department of Aeronautics & Astronautics, Wright-Patterson AFB, OH, 45433, United States (nathan.boone@afit.edu)

†PhD, Assistant Professor, Air Force Institute of Technology, Department of Aeronautics & Astronautics, Wright-Patterson AFB, OH, 45433, United States (robert.bettinger@afit.edu)

2. METHODOLOGY

The following sections provide the details of the models used to generate lunar trajectories, determine the properties of debris particles resulting from a catastrophic spacecraft explosion, and determine the risks to other spacecraft from debris. The parameters of the debris simulations are also discussed.

2.1 Lunar Trajectory Model

To support this research effort, a high-precision lunar orbit propagator was developed. This propagator includes the non-spherical nature of the Moon's gravitational field as well as the gravitational influences of the Earth and Sun. The lunar gravitational acceleration was determined using the GRAIL GRGM1200A lunar gravity model [5], truncated to degree and order 50. According to Song et al. [6], a 50×50 gravity model is sufficient to precisely model low lunar orbits over long time periods. For the accelerations due to third-body perturbations, the positions of the Earth and Sun were obtained from the JPL DE421 planetary ephemerides [7]. The accelerations of the Sun and Earth were calculated by employing the $f(q)$ method to calculate the third-body disturbing function described by Battin [8]. After summing all accelerations, the positions and velocities of particles were obtained through numerical integration using an explicit Runge-Kutta method of order 5(4).

All trajectory simulations were conducted in the "Moon Inertial" reference frame, which is described in the documentation for NASA's GMAT tool [9]. The transformation matrix from the Earth's Mean Equator and North Pole of J2000 (EME2000) to the Moon Inertial frame is:

$$[ROT]_{EME2000}^{MoonInertial} = \begin{bmatrix} 0.998496505205088 & 4.993572939853833 \times 10^{-2} & -2.260867140418499 \times 10^{-2} \\ -5.481540926807404 \times 10^{-2} & 0.909610125238044 & -0.411830900942612 \\ 0.000000000000000 & 0.412451018902688 & 0.910979778593430 \end{bmatrix} \quad (1)$$

The lunar body-fixed frame used for the lunar gravity model was the lunar Principal Axis (PA) frame [10]. The transformation matrix from the EME2000 frame to the PA frame depends on the orientation of the Moon. The lunar libration angles ϕ , θ , and ψ were obtained from the JPL DE421 planetary ephemerides, and the rotation matrix from the EME2000 frame to the PA frame was then calculated using a 3-1-3 Euler angle rotation sequence [6]:

$$[ROT]_{EME2000}^{PA} = R_3(\psi)R_1(\theta)R_3(\phi) \quad (2)$$

R_1 and R_3 are the standard 1 and 3 rotation matrices, respectively. Calculating the rotation matrix gives the following:

$$[ROT]_{EME2000}^{PA} = \begin{bmatrix} \cos \psi \cos \phi - \sin \psi \cos \theta \sin \phi & \cos \psi \sin \phi + \sin \psi \cos \theta \cos \phi & \sin \psi \sin \theta \\ -\sin \psi \cos \phi - \cos \psi \cos \theta \sin \phi & -\sin \psi \sin \phi + \cos \psi \cos \theta \cos \phi & \cos \psi \sin \theta \\ \sin \theta \sin \phi & -\sin \theta \cos \phi & \cos \theta \end{bmatrix} \quad (3)$$

A variety of coordinate transformations were required in the orbit propagator. The positions of particles were converted to the PA frame prior to applying the lunar gravity model, and then the resulting lunar gravitational acceleration in the PA frame was converted back to the coordinates of the Moon Inertial frame. Coordinate transformations were also required when implementing third-body perturbations, since the JPL planetary ephemerides are provided in the EME2000 frame. The positions of the particles were converted to the EME2000 frame to calculate the third-body accelerations, and then the third-body accelerations in the EME2000 frame were converted back to the Moon Inertial frame.

Lunar trajectories generated using this model compare favorably with those generated with GMAT. Fig. 1 and Fig. 2 compare the perilune over time for simulation of a 110-km prograde circular lunar orbit between GMAT and the lunar propagator developed for this research (lunarProp). The difference in perilune values between the two propagators is minimal, with a difference of less than one meter after one day and a difference of approximately nine meters after one month.

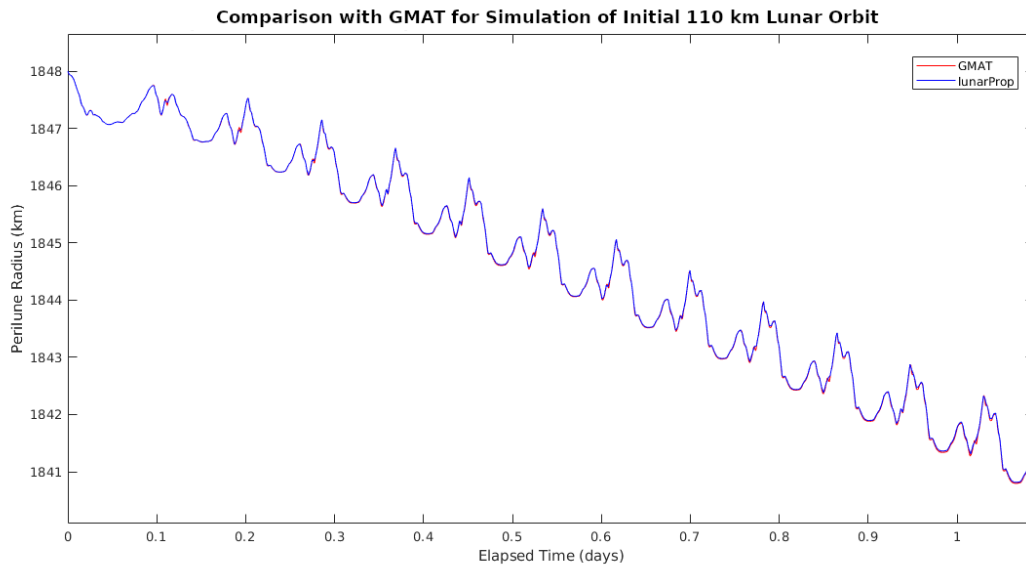


Fig. 1: Perilune Radius Comparison Between Lunar Propagator and GMAT, One Day

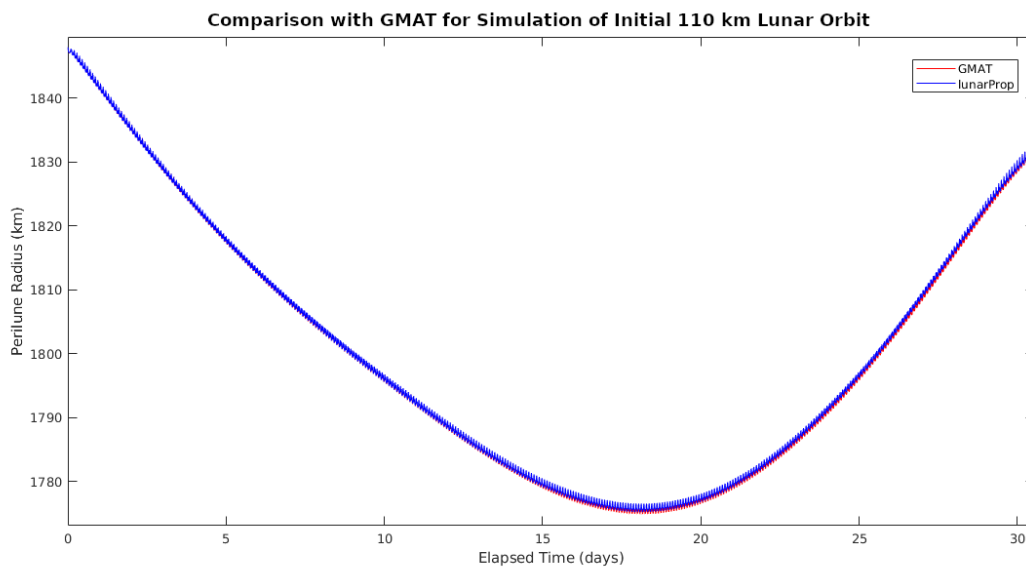


Fig. 2: Perilune Radius Comparison Between Lunar Propagator and GMAT, One Month

2.2 Catastrophic Spacecraft Mishap Model

Debris was assumed to be generated by a catastrophic battery explosion suffered by a small spacecraft with a 50 kg mass. The statistical catastrophic spacecraft mishap model developed by Boone and Bettinger [11] based on the NOAA 16 satellite battery explosion was used to determine the particle masses and velocities resulting from the explosion. In this model, all particle masses are generated by selecting random numbers from a lognormal distribution with mean of -1.7285 and standard deviation of 1.4511. Given a constant value for particle kinetic energy (KE), the particle speed can be calculated from particle mass as:

$$v = \sqrt{\frac{2}{m} KE} \quad (4)$$

A particle kinetic energy of about 580 J was used based on the median kinetic energy of particles released from the NOAA 16 battery explosion [11]. Although the spacecraft for the present study is much smaller than the NOAA 16, the properties of the explosion were assumed to be proportional to the NOAA 16 explosion. This means that the total kinetic energy released by the explosion is smaller, but fewer particles are also released, so the kinetic energy per particle is the same. After calculating the scalar particle speeds using Eq. (4), particles were assigned a random direction for their velocity vector to represent an omnidirectional explosion.

2.3 Survivability Model

To quantify the risks resulting from the debris to other spacecraft, a survivability model similar to that used by Boone and Bettinger [11] for analyzing survivability of cislunar spacecraft was applied. The lunar spacecraft survivability model used for this study is a variation of the Poisson aircraft survivability developed by Ball [12]. In this model, the debris number density ρ within a spherical “danger zone” with volume V_{DZ} surrounding a notional spacecraft threatened by debris was used to calculate the probability of hazard to the notional spacecraft. A smaller spherical region called the “hazard zone” with volume V_{HZ} bounds this notional spacecraft, and the expected number of hits E to this hazard zone were calculated using:

$$E = \rho V_{HZ} \quad (5)$$

Any particle that enters the hazard zone sphere and would cause critical damage to the spacecraft if it struck the spacecraft was considered to significantly threaten the spacecraft and represent a “hazard.”

The probability of causing critical damage in the event of an impact is the probability of kill with a hit $P_{K|H}$. This value was calculated through a vulnerability model, which will be discussed in the next section. Given a value for $P_{K|H}$, the instantaneous probability of spacecraft hazard is expressed by:

$$P_{HZ} = 1 - e^{-EP_{K|H}} \quad (6)$$

The total probability of hazard during a simulation with a start time of t_0 and an end time of t_f is given by:

$$(P_{HZ})_t = \int_{t_0}^{t_f} P_{HZ}(t) dt \quad (7)$$

The total probability of hazard during the simulation is the main result of the lunar debris study.

Discrete sampling of debris and spacecraft positions throughout the simulation means that the closest approach to the spacecraft can sometimes be missed. Therefore, a large danger zone of radius 150 km was used to ensure that all particles that could threaten the spacecraft within the discrete time steps used in survivability calculation were identified. For example, if samples of positions are made once every minute, and the speed of a particle relative to the notional spacecraft is 2.5 km/s, a particle that would strike the spacecraft at the exact start of the time step could be as far as 150 km away from the spacecraft if its position is sampled at the end of the time step. Use of a 150 km radius danger zone helps mitigate this problem. The size of the hazard zone was set as 100 meters, which reflects uncertainty in the exact position of the spacecraft.

2.4 Vulnerability Model

The vulnerability model for calculating $P_{K|H}$ used by Boone and Bettinger [11] incorporated only particle mass. A new model for $P_{K|H}$ was developed for the present lunar debris study that incorporates both particle mass and velocity. This was accomplished through the use of ballistic limit equations, which define the impact conditions that will consistently cause failure of a spacecraft shield [13]. To generate a model for $P_{K|H}$, the following Whipple shield performance equation from Christiansen [14] was used:

$$d_c = k_l \left[t_w \left(\frac{\sigma}{40} \right)^{0.5} + C_{Ltb} \rho_b \right] [\cos(\theta)]^{-11/16} \rho_p^{-0.5} V^{-2/3} \quad (8)$$

The parameters in this equation and their assumed values are given in Table 1. The assumed shield parameters represent an aluminum Whipple shield consisting of a front bumper at a standoff distance from a rear wall, as described by Christiansen [13]. The projectiles were assumed to represent aluminum debris particles, so the diameter of the debris particles d_p can be calculated from the mass.

Table 1: Parameters in Ballistic Limit Equation

Parameter Symbol	Meaning	Assumed Value
d_c	Critical projectile diameter causing shield failure (cm)	Calculated through Eq. 8
d_p	Actual projectile diameter (cm)	Calculated from average mass of particles in danger zone
θ	Impact angle measured relative to surface normal	Random variable, limited to $0 \leq \theta \leq 65^\circ$
V	Projectile speed (km/s)	Average speed of particles in danger zone relative to spacecraft
ρ_p	Density of projectile (g/cm^3)	2.70
t_w	Shield rear wall thickness (cm)	0.32
t_b	Shield bumper thickness (cm)	0.127
ρ_b	Shield bumper density (g/cm^3)	2.70
σ	Shield rear wall yield stress (ksi)	57
k_l	Empirical constant	1.9
C_L	Empirical constant (cm^3/g)	0.37

Failure of the shield occurs when the diameter of the projectile that strikes the shield exceeds the critical diameter for the impact, i.e., $d_p > d_c$. The critical diameter depends on the projectile velocity and impact angle, and the projectile diameter depends on the projectile's mass. For this research, the average velocity and mass of particles within the danger zone was known from the debris simulation and could be used to calculate d_c and d_p . However, it is difficult to determine the expected angle of impact with the spacecraft due to uncertainties in the exact trajectories of particles in the danger zone. Therefore, the impact angle was represented using a random variable.

For a cubic spacecraft, the distribution of observed impact angles is likely to be non-uniform, even with projectiles moving around the spacecraft randomly in all directions. Particles are more likely to strike the spacecraft at impact angles close to normal due to the larger area available to hit when compared to glancing impacts, which require a projectile to strike a very small sliver of area to hit the spacecraft. The probability of striking a given face (and thus having a certain impact angle) may be calculated using the ratio of the presented size of that face when compared to all other faces available to hit. Calculating impact angle probabilities for a two-dimensional case where particles approach a square spacecraft at all angles uniformly between 0 and 360° and then conducting a Monte Carlo simulation leads to the distribution of impact angles shown in Fig. 3. This distribution of impact angles was used as the distribution for the impact angle random variable θ in the ballistic limit equation. Note that impact angles above 65° were set equal to 65° in the ballistic limit equation due to an increase in shield damage for highly oblique impacts, as recommended by Christiansen [13][14].

The probability of shield failure was calculated using the fraction of impact angles that caused failure of the shield for a given projectile mass and velocity according to the ballistic limit equation in Eq. 8. The average masses and velocities of particles in the danger zone were used as the projectile mass and velocity, respectively. A failure of the shield does not necessarily mean the spacecraft will suffer critical damage, so $P_{K|H}$ was calculated by multiplying the probability of shield failure by 50%.

The variation in the resulting $P_{K|H}$ model with particle mass and velocity is shown in 4. Note that $P_{K|H}$ does not exceed 50%. The jumps in the $P_{K|H}$ curves are a result of the impact angle restriction used by Christiansen [13][14]. When oblique impacts at angles greater than 65° become capable of penetrating the spacecraft shield, all remaining impact angles between 65° and 90° will also penetrate the shield, so the $P_{K|H}$ curve jumps up to its maximum value of 50%. The shapes of the curves are quite similar to the mass-dependent logistic curve model from [11].

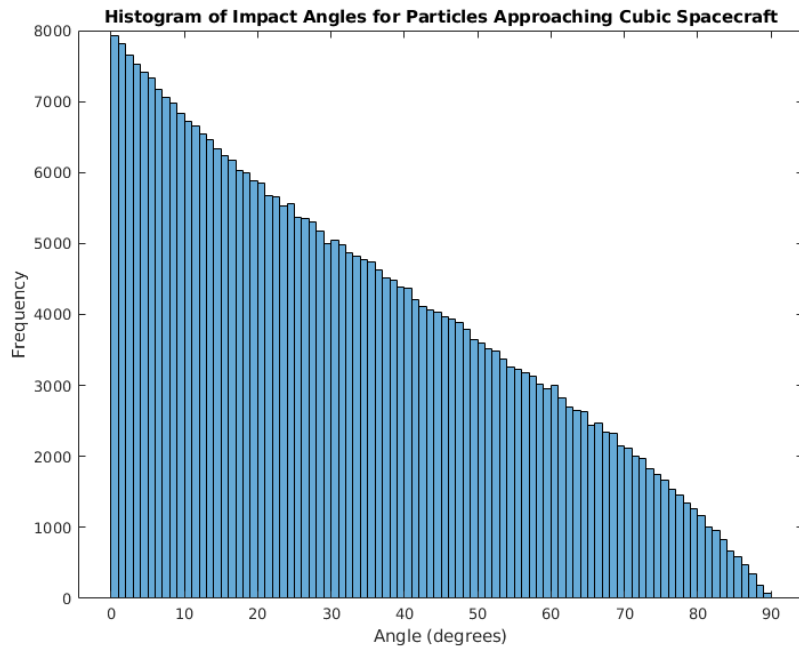


Fig. 3: Histogram Showing Distribution of Impact Angles in Monte Carlo Simulation

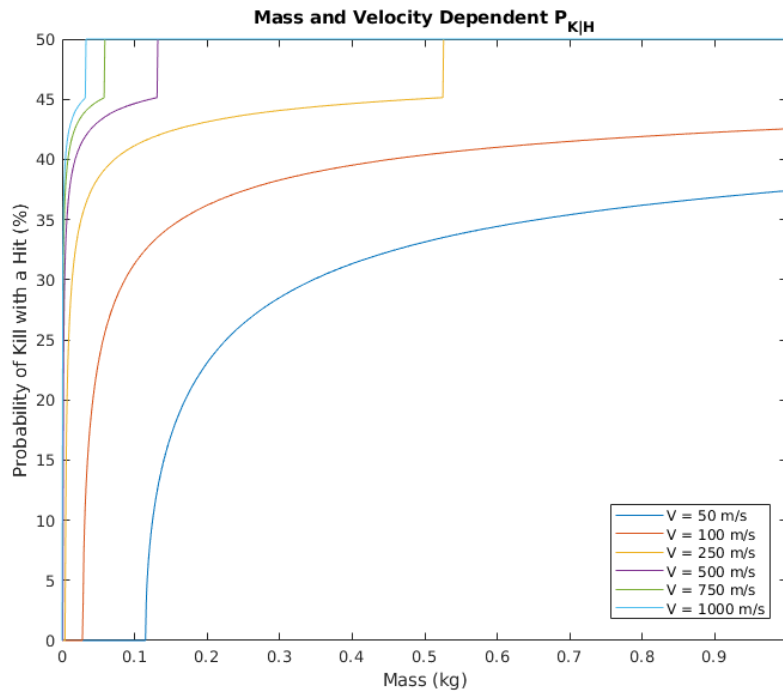


Fig. 4: Variation in Ballistic Limit Vulnerability Model with Particle Mass and Velocity

2.5 Simulation Parameters

The spacecraft that suffers the catastrophic mishap was assumed to be traveling along a circular 100-km polar lunar orbit at the time of the mishap. This orbit is very similar to the orbit used by the Japanese SELENE spacecraft [15]. Four catastrophic mishaps were simulated at four different initial positions along this orbit. The state of the spacecraft in the Moon Inertial frame just prior to the mishap for each run is provided in Table 2, and the orbital positions at the time of the mishap are shown in Fig. 5.

Table 2: Initial State of Spacecraft that Suffers Mishap for Each Run

Run	t_0 (s)	x_0 (km)	y_0 (km)	z_0 (km)	\dot{x}_0 (km/s)	\dot{y}_0 (km/s)	\dot{z}_0 (km/s)
1	0	-1838	0	0	0	0	1.633237491025757
2	0	0	0	1838	1.633237491025757	0	0
3	0	1838	0	0	0	0	1.633237491025757
4	0	0	0	-1838	-1.633237491025757	0	0

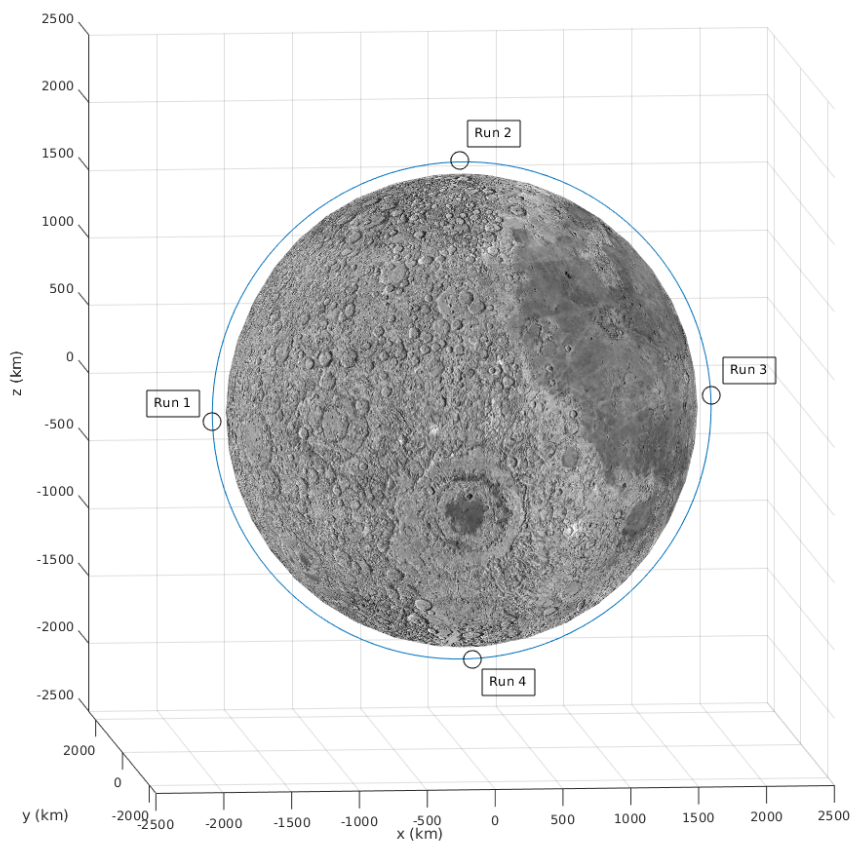


Fig. 5: Location of Catastrophic Mishap for Each Simulation Run

The spacecraft for which debris risks are determined (the “notional spacecraft”) travels along a retrograde 110-km circular lunar orbit, which is similar to the lunar orbit used by the Apollo missions [4]. The orbit was assumed to remain unchanged throughout the debris simulation, so trajectory simulation for the notional spacecraft was conducted using the Two-Body Problem. The notional spacecraft begins each run with the same position and velocity, as shown in Table 3.

Table 3: Initial State of Notional Spacecraft for Each Run

Run	t_0 (s)	x_0 (km)	y_0 (km)	z_0 (km)	\dot{x}_0 (km/s)	\dot{y}_0 (km/s)	\dot{z}_0 (km/s)
1	0	-1848	0	0	0	1.628812564197791	0
2	0	-1848	0	0	0	1.628812564197791	0
3	0	-1848	0	0	0	1.628812564197791	0
4	0	-1848	0	0	0	1.628812564197791	0

The start time of the debris simulation was set to 1 January 2040 at 00:00:00 UTC, and the stop time was 1 February 2040 00:00:00 UTC. The catastrophic mishaps occur at the simulation start time. The states of debris particles were reported once every 60 seconds during the one-month simulation, and then the trajectories of the debris particles served as the input to the survivability model.

3. RESULTS

3.1 Debris Trajectories

Snapshots of the propagation of debris throughout the simulation for Run 1 are shown in Fig. 6. The red dots in the images represent the debris particles, and the blue orbit line represents the orbit of the notional spacecraft. Run 1 resulted in 98 simulated debris particles.

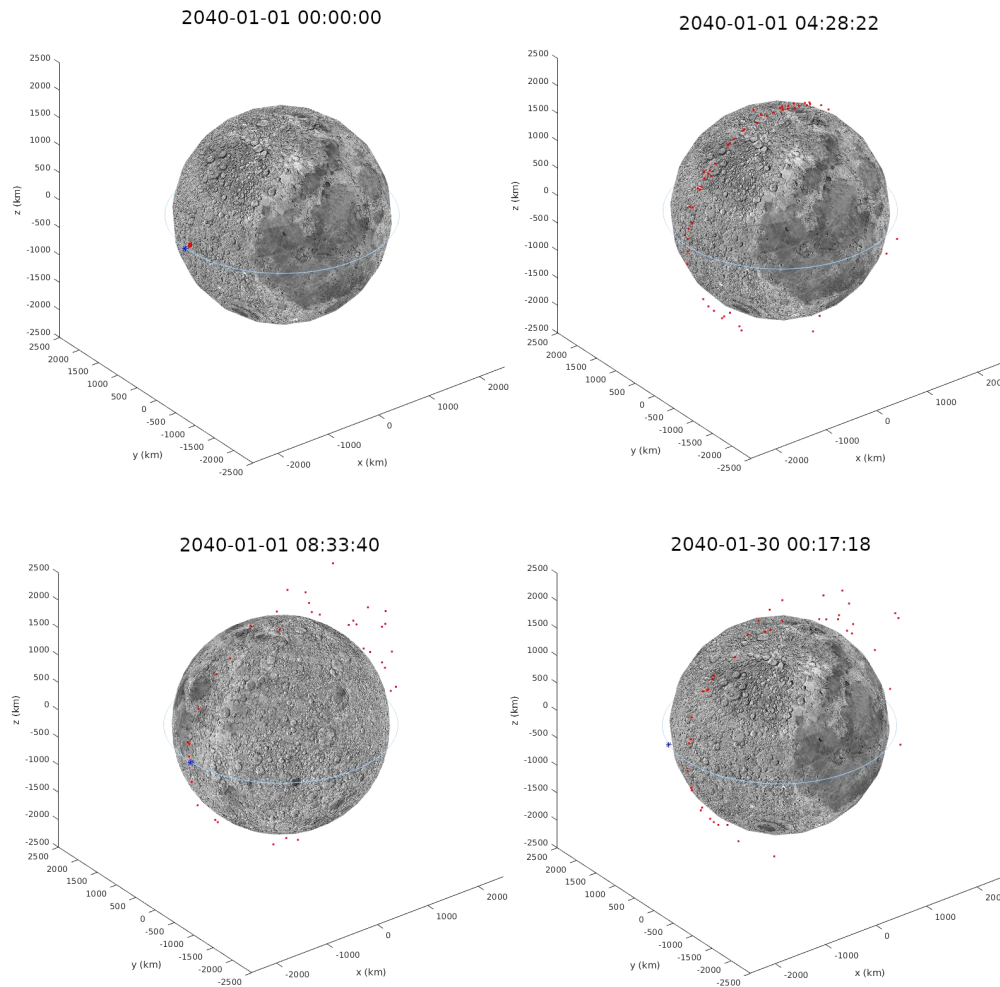


Fig. 6: Snapshots of Run 1 Debris Propagation

As shown in Fig. 6, within approximately two days after the explosion, the debris cloud had stretched to fill the circumference of the original polar orbit. A “pinch point” formed at the location of the explosion through which the debris particles passed with each orbit around the Moon. This phenomenon is commonly observed in studies of debris-generating events in Earth orbits [16]. On the opposite side of the Moon from the pinch point, there was a large spread in the orbital altitudes of the debris particles. Particles which were given significant change in velocity (ΔV) in the prograde direction had high apolunes (some as high as 4,000 km) 180° around the Moon from the pinch point, while particles that received less ΔV or retrograde ΔV had lower apolunes. The non-spherical nature of the lunar gravitational field generally resulted in periodic cycles in the orbital elements for the debris particles.

The debris simulation for the other three runs yielded similar results. Run 2 resulted in 93 simulated debris particles, Run 3 resulted in 115 debris particles, and Run 4 resulted in 114 debris particles. The main difference in the simulation runs was the location of the pinch point, which was always at the location of the explosion. The greatest variation in the orbital altitudes was always 180° around the Moon from the pinch point.

3.2 Threats to Notional Lunar Spacecraft

The total probabilities of hazard to the notional spacecraft for the four one-month simulations are shown in Table 4. All runs had very similar total P_{HZ} values, but the risk was slightly greater for Run 4. Run 1 had high instantaneous P_{HZ} values at the start of the simulation due to the proximity of the notional spacecraft to the location of the explosion, but the instantaneous P_{HZ} quickly dropped to levels typical of other runs. Although the notional spacecraft repeatedly passed through the pinch point with each orbit of the Moon for Runs 1 and 3, this did not appear to lead to a higher total probability of hazard. This may reflect the well-dispersed nature of the debris cloud around the circumference of the Moon.

Table 4: Results of Survivability Analysis

Run	P_{HZ} (1 Month)
1	$1.482 \times 10^{-3}\%$
2	$9.876 \times 10^{-4}\%$
3	$1.608 \times 10^{-3}\%$
4	$1.812 \times 10^{-3}\%$

These probabilities are roughly similar to collision risk probabilities from studies of debris hazards in near-Earth orbits. Although the probabilities reported in these studies use differing methodology and do not incorporate the vulnerability of spacecraft to the debris like the P_{HZ} results in Table 4, they suggest that the risks to lunar spacecraft following a catastrophic mishap could be comparable to the risks posed by debris in Earth orbits. For example, McKnight and Di Pentino [17] estimated annual probabilities of collision with catalogued debris for satellites at stable locations of Geostationary Earth Orbit (GEO) of between $4 \times 10^{-7}\%$ and $5 \times 10^{-7}\%$. Oltrogge et al. [18] obtained higher annual collision probabilities of between 0.179% and 0.251% for collision with catalogued objects larger than 1 cm and between $1.3 \times 10^{-2}\%$ and $1.8 \times 10^{-2}\%$ for collision with catalogued objects larger than 20 cm. Finally, Bradley and Wein [19] estimated the lifetime probability of collision with debris for a spacecraft in the most congested region of Low Earth Orbit (LEO), 900-1000 km, as $1.84 \times 10^{-2}\%$. The similarities between these values and the results in Table 4 suggest that debris may become a concern in lunar orbit, especially if the lunar environment becomes more congested in the future.

These results also show that a mishap in lunar orbit results in significantly greater risk probability than mishaps in other regions of cislunar space. Using similar methodology, Boone and Bettinger [11] found probabilities of hazard to spacecraft in the vicinity of an explosion of a 1,457 kg spacecraft of $1.81 \times 10^{-8}\%$ over 50 days for a mishap at the L_1 Lagrange point, $4.314 \times 10^{-8}\%$ over one year for a mishap at the L_4 Lagrange point, and $6.377 \times 10^{-8}\%$ over one year for a mishap at the L_5 Lagrange point. The probabilities of hazard obtained in the present study are far higher, despite a smaller mishap and a shorter simulation, because the gravity well of the Moon confines the debris to a small region following the explosion. This leads to a greater risk to other spacecraft operating in the vicinity of the mishap.

A plot of the instantaneous P_{HZ} throughout the simulation for the run that resulted in the greatest P_{HZ} , Run 4, is shown in Fig. 7. The number of particles in the danger zone and the average mass and velocity of those particles throughout the simulation is shown in Fig. 8. For all runs, the risk does not noticeably decrease during the 31-day simulation.

This indicates that the debris hazard would likely continue for much longer than 31 days, creating long-term hazards to spacecraft operating in lunar orbit.

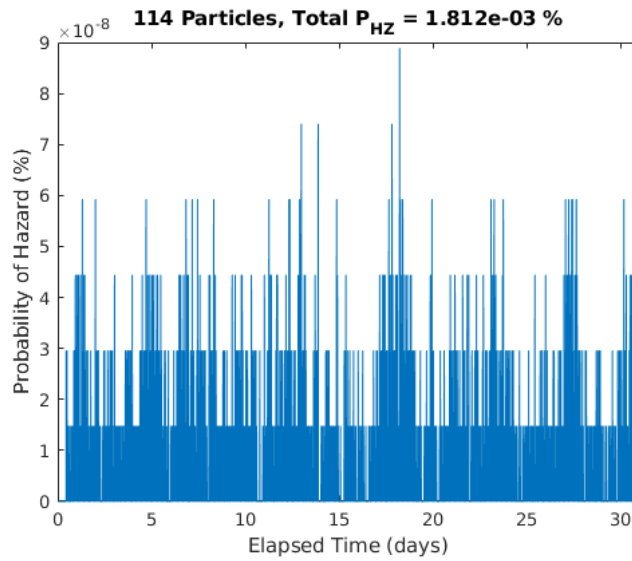


Fig. 7: Probability of Hazard Over Time for Run 4

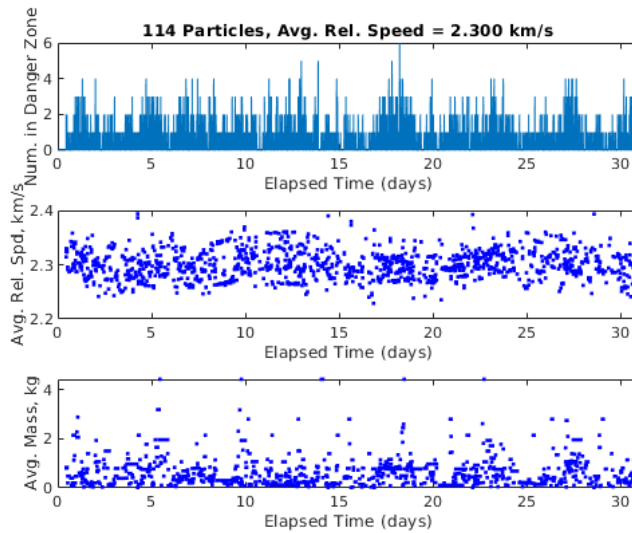


Fig. 8: Statistics For Particles in the Danger Zone Over Time for Run 4

For each run, the overall average velocity of the debris particles in the danger zone relative to the notional spacecraft was very close to 2.31 km/s, which was the difference in velocity between the notional spacecraft’s orbit and the initial pre-explosion polar lunar orbit. This is expected because the explosion adds random velocity vectors to the original velocity vector, so the average velocity across all particles remains close to the original velocity vector. According to the vulnerability model developed in Section 2.4, impacts at this velocity will penetrate the spacecraft’s Whipple shield for all but very small particles. As shown in the $P_{K|H}$ model plot in Fig. 4, this means that $P_{K|H}$ was near 50% throughout the simulation. This 50% $P_{K|H}$ represents the probability that a particle will strike a mission-critical component of the spacecraft after penetrating the Whipple shield, causing complete failure of the spacecraft.

3.3 Lunar Surface Impacts

An average of 42 debris particles had impacted the lunar surface by the end of the one-month simulation across the four runs. Fig. 9 shows the locations of the impacts on the lunar surface for each of the simulation runs. Most particles impacted within one orbit of the mishap, creating a line of impacts extending from the location of the mishap on the Moon's surface.

The lack of impacts beyond the first orbit causes the probability of hazard to remain relatively stable over time, as was shown in Fig. 7. It is likely that most of the debris would eventually decay to the lunar surface due to the non-spherical nature of the Moon's gravitational field, but this did not occur in large numbers by the end of the simulation. Song et al. [6] found that a spacecraft in a 100-km circular polar lunar orbit decayed after about 160 days, so simulations of this length would likely observe more debris particles decaying to the lunar surface. However, the very high apolunes of some particles following the mishap could greatly increase the time required to decay to the lunar surface. Additional studies with longer simulation times are needed to characterize the longevity of debris in lunar orbit following a catastrophic spacecraft mishap.

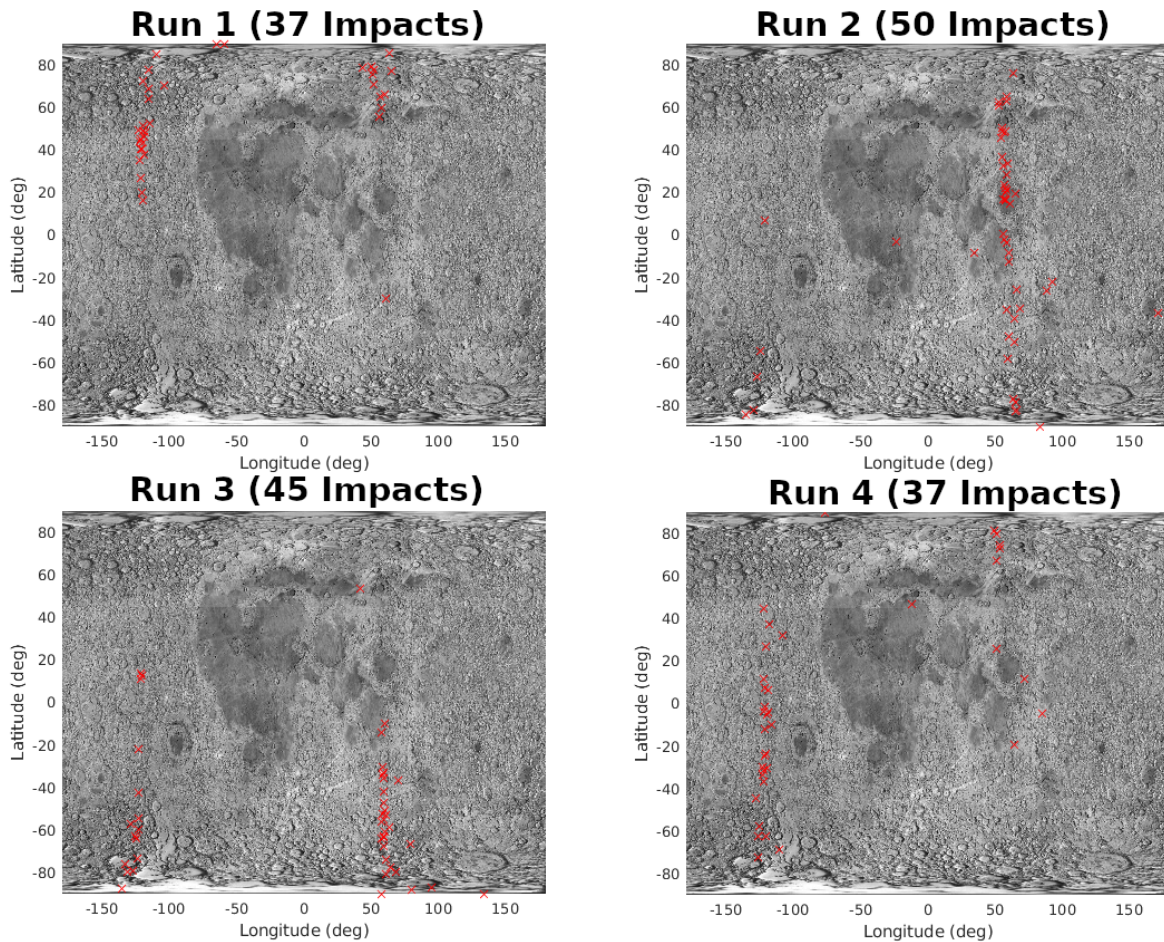


Fig. 9: Lunar Impacts for Each Simulation Run

4. CONCLUSION

This research analyzed the effects of a catastrophic mishap suffered by a spacecraft initially in a circular 100-km polar lunar orbit. The probability that a debris particle would significantly threaten a notional spacecraft in an Apollo-like equatorial lunar orbit during the one-month simulation was an average of $1.472 \times 10^{-3}\%$ across the four simulation runs. While low, this probability would likely create some concern in a real-world scenario, and it may raise the

risk from debris collision in lunar orbit to levels comparable to the risk in Earth orbits. Additionally, the risk did not diminish noticeably after one month, likely indicating potential long-term debris hazards to lunar spacecraft from the mishap. The results of this study demonstrate the need to consider debris mitigation strategies in lunar orbit, especially as more spacecraft begin to operate in this orbital environment.

Future studies of lunar debris could better characterize the risks from a catastrophic mishap by simulating a mishap that generates more debris particles, simulating the particles for longer periods of time, varying the initial lunar orbit of the spacecraft that suffers the mishap, and studying the risk to notional spacecraft in other types of lunar orbits. Longer simulation time periods would enable an understanding of the longevity of lunar debris, which would be important to understand the likelihood of accumulation of debris in lunar orbit over time. It becomes more important to fully evaluate the risks that could be posed by artificial lunar debris as crewed lunar operations begin over the next decade.

5. REFERENCES

- [1] National Aeronautics & Space Administration. The moon. Available at <https://nssdc.gsfc.nasa.gov/planetary/planets/moonpage.html>.
- [2] Leonard David. US military eyes strategic value of earth-moon space. Available at <https://www.space.com/us-military-strategic-value-earth-moon-space.html> (29 Aug 2019).
- [3] Donald J. Kessler and Burton J. Cour-Palais. Collision frequency of artificial satellites: The creation of a debris belt. *Journal of Geophysical Research*, 83(A6):2637–2646, 1978.
- [4] James Meador. Long-term orbit stability of the Apollo 11 “Eagle” lunar module ascent stage. *Planetary and Space Science*, 205, 2021.
- [5] National Aeronautics and Space Administration. Lunar gravity field: GRGM1200A. Available at <https://pgda.gsfc.nasa.gov/products/50>.
- [6] Young-Joo Song, Sang-Young Park, Hae-Dong Kim, and Eun-Sup Sim. Development of precise lunar orbit propagator and lunar polar orbiter’s lifetime analysis. *Journal of Astronomy and Space Sciences*, 27(2):97–106, 2010.
- [7] William M. Folkner, James G. Williams, and Dale H. Boggs. The planetary and lunar ephemeris DE 421. IPN Progress Report 42-178, 15 Aug 2009.
- [8] Richard H. Battin. *An Introduction to the Mathematics and Methods of Astrodynamics, Revised Edition*. American Institute of Aeronautics and Astronautics, 1999.
- [9] Steve Hughes. General Mission Analysis Tool (GMAT) technical specifications. NASA Technical Reports Server (1 Jan 2007).
- [10] National Aeronautics and Space Administration. A standardized lunar coordinate system for the Lunar Reconnaissance Orbiter and lunar datasets. Available at <https://lunar.gsfc.nasa.gov/library/LunCoordWhitePaper-10-08.pdf> (1 Oct 2008).
- [11] Nathan R. Boone and Robert A. Bettinger. Cislunar debris propagation following a catastrophic spacecraft mishap. In *Proceedings of the 2021 AIAA SciTech Forum*, 2021.
- [12] Robert E. Ball. *The Fundamentals of Aircraft Combat Survivability Analysis and Design*. American Institute of Aeronautics and Astronautics, 2003.
- [13] E. L. Christiansen. Design and performance equations for calculating spacecraft vulnerability to low Earth orbit debris. *International Journal of Impact Engineering*, 14(1–4):145–156, 1993.
- [14] E. L. Christiansen. Meteoroid/debris shielding. National Aeronautics and Space Administration, 2003.
- [15] M. Kato, S. Sasaki, K. Tanaka, Y. Iijima, and Y. Takizawa. The Japanese lunar mission SELENE: Science goals and present status. *Advances in Space Research*, 42(2):294–300, 2008.
- [16] Joel D. Slotten. Examination of debris cloud density resulting from precession of argument of perigee due to J2 effect. In *Proceedings of the 7th European Conference on Space Debris*, 2017.
- [17] Darren S. McKnight and Frank R. Di Pentino. New insights on the orbital debris collision hazard at GEO. *Acta Astronautica*, 85:73–82, 2013.
- [18] D. L. Oltrogge, S. Alfana, C. Law, A. Cacioni, and T. S. Kelso. A comprehensive assessment of collision likelihood in Geosynchronous Earth Orbit. In *Proceedings of the 68th International Astronautical Conference*, 2017.
- [19] Andrew Bradley and Lawrence Wein. Space debris: Assessing risk and responsibility. *Advances in Space Research*, 43:1372–1390, 2009.